

Effective Magnetic Switching of THz Signal in Planar Structured Spintronic Emitters

Evgeny A. Karashtin^{1,2,*}, Nikita S. Gusev¹, Maksim V. Sapozhnikov^{1,2}, Pavel Yu. Avdeev³, Ekaterina D. Lebedeva³, Anastasiya V. Gorbatova³, Arseniy M. Buryakov³, and Elena D. Mishina³

¹*Institute for Physics of Microstructures RAS, Nizhny Novgorod, Russia*

²*Lobachevsky State University of Nizhny Novgorod, Nizhny Novgorod, Russia and*

³*MIREA – Russian Technological University, Moscow, Russia*

(Dated: August 2, 2024)

We demonstrate an efficient switchable spintronic THz emission from a Co(2nm)/Pt(2nm) bilayer split into a grating of micro- or nanostripes in applied external magnetic field of the order of 10mT. The THz signal is effectively emitted if the samples are magnetized perpendicular to the stripes direction and decreases upon a 90-degree rotation of a sample. The maximal 27-fold ratio of amplitude change is achieved for the sample with a $2\mu\text{m}$ width of stripes. For the samples with easy magnetization axis directed perpendicular to stripes the THz signal is linearly polarized in the direction of the stripes and abruptly switches during the sample re-magnetization process. If the easy axis is along the stripes the THz source is almost switched off in a zero magnetic field.

I. INTRODUCTION

In the last decade, promising sources of THz radiation based on nanostructures consisting of nano-thick ferromagnetic layers (FM) having boundaries with nano-thick layers of a non-magnetic (usually heavy) metal (NM) have been actively studied and promoted [1–5]. The minimal effective structure consists of two layers: FM/NM. Numerous studies have shown that such structures can act as broadband THz emitters, comparable in efficiency to semiconductor analogues, ZnTe, semiconductor-based antennas (see for review [1, 3, 4, 6–8]). Besides they have the sufficient advantage because THz emission can be manipulated by magnetic field in this case [9].

When such a system is irradiated with a femtosecond high-intensity optical pulse, a bunch of hot electrons is generated. In a magnetic material, these hot electrons are spin-polarized, which results in a short pulse of “pure” spin current flowing from the FM to the NM. The spin current induces an electric (charge) current in the NM via the inverse spin Hall effect. Such a non-stationary electric current emits a short and broadband electromagnetic wave pulse corresponding to the terahertz frequency range [1]. Using this technology, THz fields of 1.5 MV/cm have already been achieved [10]. The highest efficiency of optical-to-THz conversion was obtained for double [11, 12] and triple [10, 11] layer structures.

Structures in which in-plane anisotropy is introduced make it possible to completely control the polarization of the emitted THz wave by changing magnitude of the magnetic field [13, 14]. Controlling amplitude by changing magnitude of the magnetic field while polarization remains constant has also been demonstrated in a spin valve type structure consisting of two layers of iron separated by a 4 nm thick layer of platinum with one of the iron layers being attached to antiferromagnetic IrMn layer [15]. In those structures, both Fe layers inject spin

current into Pt. Changing magnetization from parallel to antiparallel results in antiparallel or parallel charge current from opposite sides of the structure, thus providing minimal (zero) or maximal THz amplitude. The IrMn layer also emits THz waves when a spin current is injected into it from the neighboring iron layer, but an order of magnitude less efficiently than Pt [16, 17]. As a result, in [15] the ratio of THz signal intensities in the “on” and “off” modes of the device is approximately 15. In [18], modulation of THz intensity by up to 87% is achieved in On-Chip Wave-guided SiN_x/Fe/Pt/SiN_x structure. THz signal modulation is a primary area of research in THz communication, focusing on key parameters such as materials and structures, modulation depth, modulation speed, and others [19, 20]. Electrical modulation, while having shown good results, requires further improvement to achieve deeper and faster modulation. Optical modulation, on the other hand, already demonstrates excellent characteristics in these areas, but there is still room for improvement, making it a promising direction for further scientific research and development [19].

In this study, we propose a structure that provides a novel mechanism for controlling the amplitude of a THz signal from a spintronics emitter using an external magnetic field. We used a standard cobalt-platinum bilayer and etched a grating in it with a sub-wavelength period throughout the entire depth of the bilayer. This array acts as a THz antenna, where a magnetic field applied perpendicularly or parallel to the stripes allows the amplitude of the THz wave to be modulated with a high modulation depth. The efficiency of amplitude modulation has been studied depending on the width and period of the stripes, and a theoretical justification for the observed dependencies has been given.

The paper is organized as follows. In Section II we describe preparation of the samples and the experimental measurement technique. Section III compiles the experimental data for THz signal from all samples. In Section IV, the results of measurements are discussed and appropriate theory is verified showing reasonable fitting

* eugenk@ipmras.ru

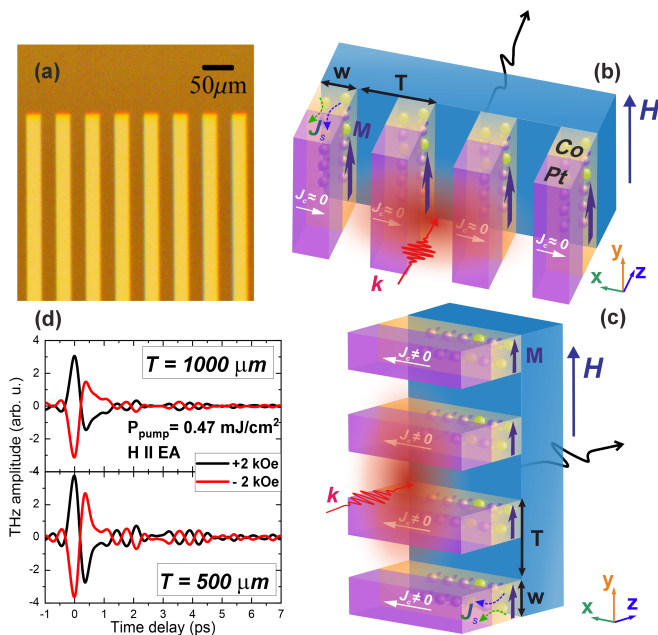


FIG. 1. (a) Optical photograph of a $50\mu\text{m}$ period grating. (b,c) Schematic representation of current (J_c) and amplitude of generated THz signal for the magnetic field applied along the stripes or perpendicular to them, respectively. (d) Typical time dependence of terahertz field emitted from the Co(2)/Pt(2) for the grating with $1000\mu\text{m}$ and $500\mu\text{m}$ period ($500\mu\text{m}$ and $250\mu\text{m}$ stripe width, respectively).

parameters.

II. METHODS AND SAMPLES

The spintronic terahertz emitters are Co(2)/Pt(2) bilayer films (hereafter, thickness is in nm, order of layers is from substrate) grown on quartz substrates by magnetron sputtering. An external magnetic field of approximately 1kOe was applied during growth in order to induce a uniaxial anisotropy in the sample plane. Details of growth technology may be found elsewhere [21]. The $1\text{cm} \times 1\text{cm}$ -size gratings with microns to hundreds of microns period (4, 50, 100, 300, 500, $1000\mu\text{m}$) and $1/2$ filling factor are then made from these films by optical lithography (Figure 1(a)). We also make a sample with $8\mu\text{m}$ period and $3/4$ filling factor ($6\mu\text{m}$ stripe width). Samples of periodic spintronic emitters with anisotropy both along the easy axis (E.A.) relative to the stripes and across the stripes were manufactured.

Sample planar structure characterization was performed by optical microscopy. Magnetic properties were checked by longitudinal magneto-optical Kerr rotation (MOKE) investigation with the use of He-Ne laser with the wavelength of 630 nm . THz emission measurements were conducted by using a standard THz time-domain spectroscopy method. A Ti:Sapphire laser with an amplifier system generated pulses with a central wavelength

of 800 nm , repetition rate of 3kHz , and pulse duration of 35fs . Samples of spintronic THz emitters were placed in a constant external magnetic field of up to 2kOe , created by an electromagnet. A magnetic field was applied along the Y-axis of the laboratory coordinate system (Figure 1(c)). This study considered two geometries for magnetic field application: magnetizing samples along an easy axis $H \parallel \text{E.A.}$ and along a hard axis $H \parallel \text{H.A.}$. These geometries are achieved by a 90-degree rotation of a sample in the laboratory coordinate system. This is shown schematically in Figure 1(b,c) for structures in which the easy axis is aligned along the direction of the stripes. These pictures also illustrate the mechanism of THz generation due to ISHE in both configurations (arrows indicate the directions of the spin current J_s injected from the ferromagnetic layer into the layer of non-magnetic Pt and the charge current J_c generated as a result of ISHE).

The generated THz signal was focused onto a nonlinear optical crystal, ZnTe, using a system of parabolic mirrors. To detect the THz signal, a standard electro-optical sampling technique was employed with a setup that included the ZnTe detector, a quarter-wave plate, a Wollaston prism, and a balanced photodetector. The polarization of the pump and probe beams was aligned parallel to the X-axis of the laboratory coordinate system (Figure 1(c)) and the ZnTe axis (-110). The laser spot size on the samples was 3mm at the FWHM level, corresponding to a pump energy density of 0.47mJ/cm^2 . A wire-grid polarizer installed in the THz radiation path, along with the THz polarization-sensitive ZnTe, enabled the analysis of the THz radiation polarization. All measurements presented in this work were performed for the Ex component of the THz field. A more detailed description of the THz detection setup can be found in Ref. [22].

III. EXPERIMENTAL RESULTS

All samples are verified via the MOKE measurements along and perpendicular to the easy axis. Typical MOKE curves are shown in Figure 2 for the initial film and a grating with $2\mu\text{m}$ wire width. For micron-sized stripes, the easy axis (E.A.) is along the magnetic field applied during the sample growth regardless of the stripe direction. The magnetization reverses abruptly in $20-40\text{Oe}$ if the magnetic field is applied along the easy axis for all the samples. For the magnetic field applied along the hard axis (H.A.) the saturation is reached at approximately 100Oe .

We perform time dependence of THz field amplitude for the setup when the grating is irradiated by an optical pump from front (sample) and back (substrate) side. The main quantitative difference is the magnitude of signal due to different absorption coefficients for optical and THz signal in a quartz substrate. Note that the results are qualitatively the same both for front and back side. Typical result for irradiation from front side is shown in

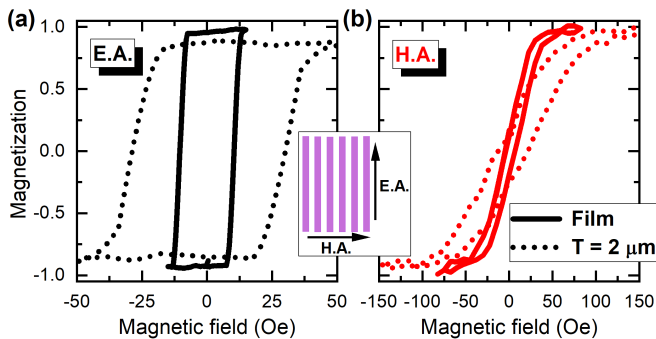


FIG. 2. MOKE hysteresis loop along (a) the easy axis (E.A.) and (b) the hard axis (H.A.) for the initial Co(2)/Pt(2) film (solid line) and for the sample with a $4\mu\text{m}$ period grating and a $2\mu\text{m}$ stripe width (dashed line). The inset shows the orientation of easy axis with respect to the stripe direction.

Figure 1(d) for $1000\mu\text{m}$ and $500\mu\text{m}$ grating period with $1/2$ filling factor and close geometry.

Figure 3 shows the hysteresis loop for the THz signal when an external magnetic field is applied either along or perpendicular to the easy axis for different grating periods. The hysteresis loop is constructed as follows. The THz signal is measured at a delay position of 0 ps , which corresponds to the peak maximum (as shown in Figure 1(d)). Then, at this position, a magnetic field is applied, and the corresponding THz amplitude is recorded for each value of the magnetic field. Typically, the THz signal polarized in the direction perpendicular to the magnetic field applied to the sample is recorded. We designate this usual signal polarization as X-polarization. In the left column of Figure 3, the hysteresis loops are shown for samples with the E.A. perpendicular to the stripes at grating periods of (a) $1000\mu\text{m}$, (b) $50\mu\text{m}$, (c) $8\mu\text{m}$. In the right column of Figure 3, the hysteresis loops are shown for samples with the E.A. parallel to the stripes at grating periods of (d) $300\mu\text{m}$, (e) $100\mu\text{m}$, (f) $8\mu\text{m}$. The insets at the top of Figure 3 show the orientation of the easy axis (E.A.) and the hard axis (H.A.) relative to the direction of the grating. The black curves correspond to magnetization along the easy axis (E.A.), while the red curves correspond to magnetization along the hard axis (H.A.).

One can straightforwardly see that the signal amplitude in a saturating magnetic field depends on whether the sample is magnetized along or perpendicular to the stripes while the loop shape depends on the direction of easy axis with respect to grating orientation. The decrease in THz signal amplitude after the samples are magnetized along the hard axis and then the magnetic field is turned off is due to the change of the magnetic state: the samples are split into magnetic domains in which the magnetization turns along local easy axis direction. Non-zero remanent magnetization is due to a non-uniform polycrystalline structure of the sample.

We also measure the other linear polarization (which we denote as Y-polarization) of THz signal (see Supple-

mentary Materials) where the polycrystalline structure of the sample is even more pronounced. The main feature of these measurements is that for narrow stripes the Y-polarized signal is very small when the magnetic field is applied perpendicular to the stripes. This matches the fact that these samples poorly emit THz signal when magnetized along the stripes. Thus almost one linear polarization of the THz signal is emitted well from narrow stripes; the amplitude of this signal can be effectively controlled by the direction of applied magnetic field with respect to the stripes orientation.

To conclude this section, Figure 4 shows the THz signal from the sample with $2\mu\text{m}$ -wide stripes and a period of $4\mu\text{m}$, with the easy axis aligned along the stripes. In Figure 4(a), the time-domain THz signal is shown for different magnetic field orientations: $+0.4\text{ kOe}$ and -0.4 kOe along the hard axis (H.A.) and $+0.4\text{ kOe}$ and -0.4 kOe along the easy axis (E.A.). For the THz signal measurements along the easy axis (E.A.), the signal was amplified 10 times for better visibility in the plot. The blue line at 0 picoseconds corresponds to the peak maximum, as shown in Figure 4(b). In Figure 4(b), the THz peak amplitude is plotted as a function of the applied magnetic field. It can be seen that there is a drastic 27-fold difference in the signal magnitude upon a 90 -degree rotation

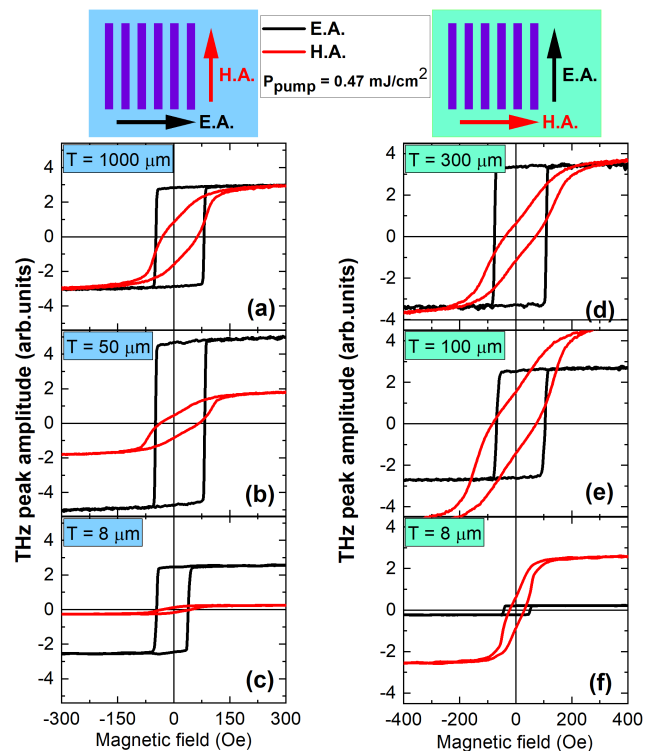


FIG. 3. THz hysteresis loop for the magnetic field along (black line) or perpendicular (red line) to easy axis for (a) $1000\mu\text{m}$, (b) $50\mu\text{m}$, (c) $8\mu\text{m}$ grating period and E.A. perpendicular to stripes and (d) $300\mu\text{m}$, (e) $100\mu\text{m}$, (f) $100\mu\text{m}$ grating period and E.A. parallel to stripes. The orientations of easy and hard axis are shown in the insets.

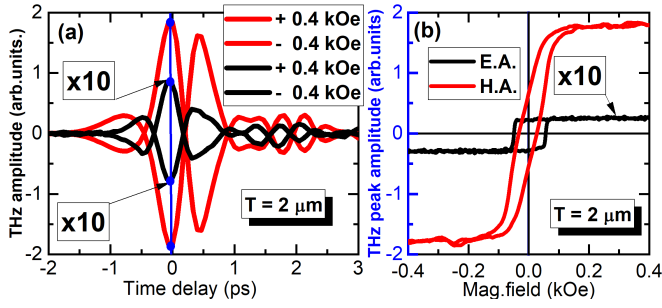


FIG. 4. (a) Time dependence of THz signal in a saturating field of $\pm 0.4 kOe$ for the sample with $2 \mu m$ wide stripes magnetized along hard axis (perpendicular to stripes) and along easy axis (parallel to stripes). (b) THz hysteresis loops and the direction of easy axis and hard axis.

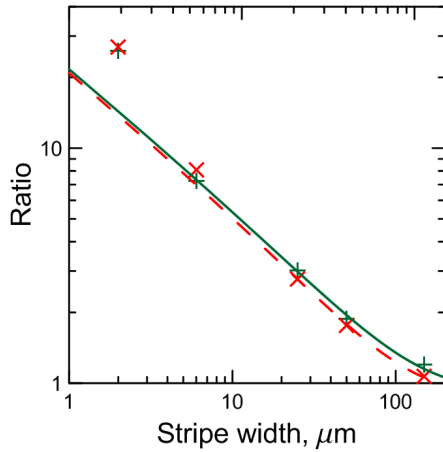


FIG. 5. THz signal ratio versus stripe width for front side (pluses) and back side (crosses) measurement. The lines represent theoretical approximation (solid line for front side, dashed line for back side).

of the sample.

IV. DISCUSSION

The results for the THz signal ratio versus the stripe width extracted from the experimental data for different stripe width from $150 \mu m$ down to $2 \mu m$ for both front and back side measurements are shown in Figure 5 (in logarithmic scale). One can see that the ratio grows as the stripe width becomes smaller, but quite slowly. Similar dependencies are observed for front side and back side measurements.

In order to provide a fit of the experimental data we develop the following theoretical model. For the sample magnetized perpendicularly to the stripes, they are supposed to be infinite. Hence the electric current flows with no charge accumulation. We suppose that the power injected into a unit square of the emitter from magnetic system p_i is constant. The electric field emitted per one

stripe is then proportional to the electric current through it: $I_{\parallel} \sim \sqrt{\frac{2p_i l^2 h}{\rho}}$, where ρ is resistivity, l, h are length and thickness of the stripe, respectively. For sample magnetization along the stripes a permanent current would split charges with the velocity of light and then stop. Since the current source provided by ISHE is alternating we ought to calculate the high-frequency conductance. It consists of active resistance determined by film conductivity and reactance mainly determined by electrical capacitance of the system. We may roughly estimate it by supposing that the charge is conducted at very thin wires with the diameter equal to the layer thickness h (Figure 6). We then calculate the energy power accumulated at such an edge in the electric field of all other edges with alternating charge sign and take into account that the electric field of the charge that lies at the metal side is screened by a factor of ξ :

$$p_c = (1 - \xi) \frac{I_{\perp}^2}{2l\omega} \text{Log} \left(\frac{L}{w} \right), \quad (1)$$

where ω is the frequency of electric current I_{\perp} , L and w are the characteristic grating width and the stripe width. Taking into account power absorption due to the wire resistance it is then easy to obtain an estimation of the electric current that emits THz signal:

$$I_{\perp} \sim \sqrt{\frac{2p_i l^2 h}{\rho + \frac{1-\xi}{\omega} \frac{h}{w} \text{Log} \left(\frac{L}{w} \right)}}. \quad (2)$$

It is then straightforward to calculate the THz signal ratio as:

$$\text{Ratio} = \frac{I_{\parallel}}{I_{\perp}} = \sqrt{1 + \frac{h}{L} \frac{1-\xi}{\rho\omega} \frac{L}{w} \text{Log} \left(\frac{L}{w} \right)}. \quad (3)$$

The results of experimental data fit with the use of (3) are shown in Figure 5 by solid (dashed) line for front (back) side configuration. Note that we use data for relatively big ($> 10 \mu m$) stripe width for the fit. The characteristic grid coherence length L is determined from the fit and is equal to $264 \mu m$ for front side measurements and $184 \mu m$ for back side ones. These values are of the same order; the difference may be attributed to sensitivity of

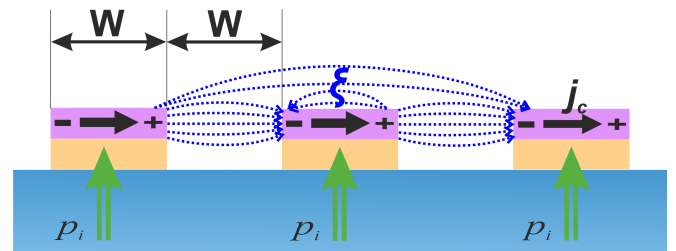


FIG. 6. A schematic view of stripes cross section. The electric charges accumulate at the boundaries and create an electric field which leads to energy accumulation.

this parameter to small deviations of experimental values caused by noise. One can note that although the real grid size is of the order of 1cm we obtain L of the order of THz signal wavelength. This is governed by the fact that equation (3) is obtained in the quasistatic approximation which works well for distances less than the wavelength. The other fitting parameter is the stripe effective resistivity ρ . Supposing that the screening parameter $\xi \ll 1$ we evaluate it from our fit as $\rho = 8 \cdot 10^{-8} \Omega \cdot m$ for measurements from both sides. Considering the structure as a parallel connection of Pt and Co conductors with the same cross section and resistivity equal to $10.6 \cdot 10^{-8} \Omega \cdot m$ and $6.2 \cdot 10^{-8} \Omega \cdot m$ respectively [23] we arrive at a very close resistivity equal to $8.4 \cdot 10^{-8} \Omega \cdot m$. Thus our rough model fits the experimental data quite well.

It is worth noting that the model (and the experiment) is almost not sensitive to the distance between stripes unless this distance is of the order of value of the stripe width w . This is explained by a logarithmic dependence of the energy stored in the accumulated charge on this distance which leads to a small constant correction under the root in (3). Indeed, the point put for $6\mu\text{m}$ stripe width in Figure 5 is measured at the $2\mu\text{m}$ distance between stripes. Although it is not used for theoretical fit it corresponds to that fit quite well. On the other hand, the ratio value equal to 27 obtained for the $2\mu\text{m}$ stripe width is slightly greater than that predicted by Equation 3 (approximately 15). This may be attributed to the fact that we do not take into account some other effects such as the circuit inductance in our model. This makes the THz signal ratio even greater.

V. CONCLUSION

In summary, we show that the planar grating that consists of stripes made of typical ferromagnet / heavy metal spintronic terahertz emitter may act as a THz source

which intensity can be effectively controlled by application of an external magnetic field: the source emits THz signal well if magnetized perpendicular to the stripes direction and much worse if magnetized along the stripes. The ratio of THz signals is approximately 27 (almost two times greater than that for a structure with two ferromagnetic layers divided by a relatively thick 4nm Pt interlayer [15]) for the stripe width $2\mu\text{m}$ which is easily achieved by optical lithography. Although the overall THz signal amplitude obtained from our samples is less than from solid films by a filling factor our method may give a greater signal than that suggested in literature [15] because of a much smaller total thickness of layers that we use. Our samples emit the THz signal linearly polarized along the stripes; thus we straightforwardly intergate a linear polarization THz antenna into the spintronic emitters.

The THz signal from the samples with crystalline anisotropy perpendicular to the stripes direction almost abruptly switches from one THz field polarization direction to an opposite one upon a remagnetization process which gives two controllable THz signal states. On the other hand, for the samples with crystalline anisotropy parallel to the stripe direction the THz field goes from a maximum in a saturating field to a very small value in zero field thus allowing to controllably achieve three states of THz signal. This opens up a possibility to create either two- or three-state controllable sources for possible use in THz logic devices [24, 25].

ACKNOWLEDGMENTS

This work was supported by Center of Excellence “Center of Photonics” funded by The Ministry of Science and Higher Education of the Russian Federation, contract 075-15-2022-316. THz measurement experiments were supported by the RSF (Grant No. 23-19-00849).

-
- [1] C. Bull, S. M. Hewett, R. Ji, C.-H. Lin, T. Thomson, D. M. Graham, and P. W. Nutter, Spintronic terahertz emitters: Status and prospects from a materials perspective, *APL Materials* **9** (2021).
 - [2] L. Cheng, Z. Li, D. Zhao, and E. E. M. Chia, Studying spin-charge conversion using terahertz pulses, *APL Materials* **9**, 070902 (2021), 10.1063/5.0051217.
 - [3] T. S. Seifert, L. Cheng, Z. Wei, T. Kampfrath, and J. Qi, Spintronic sources of ultrashort terahertz electromagnetic pulses, *Applied Physics Letters* **120**, 180401 (2022).
 - [4] A. Leitenstorfer, A. S. Moskalenko, T. Kampfrath, J. Kono, E. Castro-Camus, K. Peng, N. Qureshi, D. Turchinovich, K. Tanaka, A. G. Markelz, M. Havenith, C. Hough, H. J. Joyce, W. J. Padilla, B. Zhou, K.-Y. Kim, X.-C. Zhang, P. U. Jepsen, S. Dhillon, M. Vitiello, E. Linfield, A. G. Davies, M. C. Hoffmann, R. Lewis, M. Tonouchi, P. Klarskov, T. S. Seifert, Y. A. Gerasimenko, D. Mihailovic, R. Huber, J. L. Boland, O. Mitrofanov, P. Dean, B. N. Ellison, P. G. Huggard, S. P. Rea, C. Walker, D. T. Leisawitz, J. R. Gao, C. Li, Q. Chen, G. Valušis, V. P. Wallace, E. Pickwell-MacPherson, X. Shang, J. Hesler, N. Ridler, C. C. Renaud, I. Kallfass, T. Nagatsuma, J. A. Zeitler, D. Arnone, M. B. Johnston, and J. Cunningham, The 2023 terahertz science and technology roadmap, *Journal of Physics D: Applied Physics* **56**, 223001 (2023).
 - [5] G.-S. Park, M. Tani, J.-S. Rieh, and S. Y. Park, *Advances in Terahertz Source Technologies* (Jenny Stanford Publishing, 2024).
 - [6] T. Kampfrath, M. Battiato, P. Maldonado, G. Eilers, J. Nötzold, S. Mährlein, V. Zbarsky, F. Freimuth, Y. Mokrousov, S. Blügel, M. Wolf, I. Radu, P. M. Oppeneer, and M. Münzenberg, Terahertz spin current pulses controlled by magnetic heterostructures, *Nature Nanotechnology* **8**, 256 (2013).
 - [7] E. Y. Vedmedenko, R. K. Kawakami, D. D. Sheka,

- P. Gambardella, A. Kirilyuk, A. Hirohata, C. Binck, O. Chubykalo-Fesenko, S. Sanvito, B. J. Kirby, *et al.*, The 2020 magnetism roadmap, *Journal of Physics D: Applied Physics* **53**, 453001 (2020).
- [8] W. Wu, C. Yaw Ameyaw, M. F. Doty, and M. B. Jungfleisch, Principles of spintronic THz emitters, *Journal of Applied Physics* **130**, 091101 (2021).
- [9] D. Kong, X. Wu, B. Wang, T. Nie, M. Xiao, C. Pandey, Y. Gao, L. Wen, W. Zhao, C. Ruan, J. Miao, Y. Li, and L. Wang, Broadband spintronic terahertz emitter with magnetic-field manipulated polarizations, *Advanced Optical Materials* **7**, 1900487 (2019).
- [10] R. Rouzegar, A. L. Chekhov, Y. Behovits, B. R. Serrano, M. A. Syskaki, C. H. Lambert, D. Engel, U. Martens, M. Münzenberg, M. Wolf, G. Jakob, M. Kläui, T. S. Seifert, and T. Kampfrath, Broadband spintronic terahertz source with peak electric fields exceeding 1.5 mv/cm, *Phys. Rev. Appl.* **19**, 034018 (2023).
- [11] T. Kampfrath, A. Kirilyuk, S. Mangin, S. Sharma, and M. Weinelt, Ultrafast and terahertz spintronics: Guest editorial, *Applied Physics Letters* **123**, 050401 (2023).
- [12] A. M. Buryakov, A. V. Gorbatova, P. Y. Avdeev, E. D. Lebedeva, K. A. Brekhov, A. V. Ovchinnikov, N. S. Gusev, E. A. Karashtin, M. V. Sapozhnikov, E. D. Mishina, N. Tiercelin, and V. L. Preobrazhensky, Efficient Co/Pt THz spintronic emitter with tunable polarization, *Applied Physics Letters* **123**, 082404 (2023).
- [13] D. Khusyainov, S. Ovcharenko, M. Gaponov, A. Buryakov, A. Klimov, N. Tiercelin, P. Pernod, V. Nozdrin, E. Mishina, A. Sigov, and V. Preobrazhensky, Polarization control of thz emission using spin-reorientation transition in spintronic heterostructure, *Scientific Reports* **11**, 697 (2021).
- [14] Y. Wang, H. Cheng, W. Li, Z. Liu, X. Jia, Q. Huang, and Y. Lu, Actively switchable spintronic terahertz emission with arbitrary polarization states, *Applied Physics Letters* **124**, 091103 (2024).
- [15] M. Fix, R. Schneider, S. Michaelis de Vasconcellos, R. Bratschitsch, and M. Albrecht, Spin valves as magnetically switchable spintronic THz emitters, *Applied Physics Letters* **117**, 132407 (2020).
- [16] M. Chen, R. Mishra, Y. Wu, K. Lee, and H. Yang, Terahertz emission from compensated magnetic heterostructures, *Adv. Optical Mater.* , 1800430 (2018).
- [17] Y. Saito, F. N. Kholid, E. Karashtin, I. Pashenkin, and R. V. Mikhaylovskiy, Terahertz emission spectroscopy of exchange-biased spintronic heterostructures: Single- and double-pump techniques, *Phys. Rev. Appl.* **19**, 064040 (2023).
- [18] B. Y. Shahriar, E. Hopmann, and A. Y. Elezzabi, On-chip waveguided spintronic sources of terahertz radiation, *ACS Photonics* **10**, 518 (2023).
- [19] Z. T. Ma, Z. X. Geng, Z. Y. Fan, J. Liu, and H. D. Chen, Modulators for terahertz communication: The current state of the art, *Research* , 6482975 (2019).
- [20] W. Liu and Z. Song, Terahertz absorption modulator with largely tunable bandwidth and intensity, *Carbon* **174**, 617 (2021).
- [21] A. A. Fraerman, S. A. Gusev, L. A. Mazo, I. M. Nefedov, Y. N. Nozdrin, I. R. Karetnikova, M. V. Sapozhnikov, I. A. Shereshevskii, and L. V. Sukhodoev, Rectangular lattices of permalloy nanoparticles: Interplay of single-particle magnetization distribution and interparticle interaction, *Phys. Rev. B* **65**, 064424 (2002).
- [22] A. Buryakov, A. Gorbatova, P. Avdeev, N. Bezikonnyi, D. Abdulaev, A. Klimov, S. Ovcharenko, and E. Mishina, Controlled spintronic emitter of thz radiation on an atomically thin ws₂/silicon substrate, *Metals* **12**, 1676 (2022).
- [23] I. S. Grigoriev and E. Z. Meilikhov, eds., *Handbook of Physical Quantities* (CRC Press, Boca Raton, FL, United States, 1996).
- [24] M. Ortiz-Martinez, A. I. Hernandez-Serrano, M. A. J. Guerrero, E. Strupiechonski, and E. Castro-Camus, Logic gates for terahertz frequencies fabricated by three-dimensional printing, *J. Opt. Soc. Am. B* **37**, 3660 (2020).
- [25] Z. Wang, Z. Zhang, F. Qiu, M. Wang, W. Yang, Z. Li, X. Hu, Y. Li, X. Yan, H. Yao, and L. Liang, Design of an all-optical multi-logic operation-integrated metamaterial-based terahertz logic gate, *Opt. Express* **30**, 40401 (2022).